A Multivariable Adaptive Control Design with Applications to Autonomous Helicopters

A. S. Krupadanam [*], A. M. Annaswamy [†], and R. S. Mangoubi [‡]

Abstract

Control of autonomous helicopters in the presence of environmental and system uncertainties is a challenging task. These uncertainties not only change the dynamics of the system but the trim inputs themselves. In this paper, a viable multivariable adaptive control methodology is proposed that is applicable for general maneuvers with arbitrary speeds and high bandwidth requirements. The control design methodology achieves global stability, and is tested on a high fidelity simulation of a real life autonomous helicopter. The results indicate a satisfactory tracking performance even as the speeds and bandwidth requirements are increased well beyond hover, and as the parametric uncertainties were increased by about 20% of their nominal values.

Nomenclature

Γ	Inverse of adaptation gain matrix
Γ_1	Adaptation gain
Γ_2	Adaptation gain
Γ_3	Adaptation gain
Γ_r	Adaptation robustness matrix
Γ_{r1}	Adaptation robustness gain
Γ_{r2}	Adaptation robustness gain
Γ_{r3}	Adaptation robustness gain
η	Efficiency of Engine

[*]Maxtor Corporation, 333 South Street, Shrewsbury, MA 01545 Email: krupa@alum.mit.edu

[†]Department of Mechanical Engineering, Massachusetts Institute of Technology, Cambridge, MA 02139 Email: aanna@mit.edu

[‡]Draper Laboratory, Cambridge, MA 02139 Email: rmangoubi@draper.com

θ	Pitch attitude
Θ	System parameter vector
Θ_0	Nominal system parameter vector
Θ_c	Controller parameter matrix
$\bar{\Theta}_c^*$	Ideal controller parameter matrix
$\bar{\Theta}_c$	Augmented controller parameter matrix
Θ_s	Set of all system parameter values
λ_f	Fraction of fuel capacity remaining
ν	Observability index of plant
π_p	Monic polynomial of degree 1
ρ	Atmospheric density
ϕ	Roll attitude
$\Phi\left(t\right)$	Controller parameter error matrix
ψ	Heading angle
ω	Non-minimal representation of x_p
$\bar{\omega}$	Augmented non-minimal state representation
ω_0	Vector of unit elements
ω_i	Part of non-minimal state ω, $i = 1, ..., \nu - 1$
ω_j	Part of non-minimal state ω, $j = \nu, ..., 2\nu - 1$
Ω_{max}	Engine speed at maximum output
Ω	Angular rate of main rotor
a_1	Rotor disk pitch angle
$a_{1,FB}$	Flybar pitch angle
a_{FB}	Lift curve slope of flybar
a_{mr}	Lift curve slope of main rotor blade
a_{tr}	Lift curve slope of tail rotor blade
A	State-space representation matrix
A_p	State-space representation matrix about nominal trim

b_1 Rotor disk roll angle

$b_{1,FB}$ Flybar roll angle

b_{mr} Number of main rotor blades

b_{tr} Number of tail rotor blades

B State-space representation matrix

B_m Reference model state space representation matrix

B_p State-space representation matrix about nominal trim

c_{FB} Chord of flybar paddle

c_{mr} Chord of main rotor blade

c_{tr} Chord of tail rotor blade

C State space representation matrix

C_i Controller parameter matrix of size $m \times m$, $i = 1, ..., \nu - 1$

$C_{D0,mr}$ Zero-lift drag coefficient of main rotor blade

$C_{D0,tr}$ Zero-lift drag coefficient of tail rotor blade

$\hat{d}$ Trim error estimate

d_0 Input disturbance due to d_x and d_y

d_1 Input disturbance due to d_x and d_y

d_1 Output disturbance

d_x State disturbance

d_y Output disturbance

D_e Gear reduction ratio of main rotor

D_j Controller parameter matrix of size $m \times m$, $j = 0, ..., \nu - 1$

D_{tr} Tail rotor turns per turn of main rotor

e State error $x_p - x_m$

e_0 Quaternion element

e_1 Quaternion element

$e_1(t)$ Output error $z_p(t) - z_m(t)$

e_2 Quaternion element

e_3 Quaternion element

f System dynamics

g Gravitational Acceleration

$H_p(s)$ Hermite normal form of system transfer function matrix

I_b Flapping inertia of main rotor blade

I_{FB} Flapping inertia of flybar paddle

I_{xx} Roll axis moment of inertia

I_{yy} Pitch axis moment of inertia

I_{zz} Yaw axis moment of inertia

k_i Measure of column relative degree

K Control matrix

K_0 Controller parameter matrix of size $m \times m$

$\overline{K}_0$ Controller parameter matrix of size $m \times m$

K_p High frequency gain of $W_p(s)$

$\overline{K}_p$ High frequency gain of plant with precompensator

K_{cyc}^{fb} Flybar cyclic pitch per cyclic pitch control input

K_{fb}^{cyc} Main rotor cyclic pitch per flybar tip path deflection

K_{GE} Ground effect parameter

m Number of input and outputs of $W_m(s)$

m_e Mass without fuel

m_f Fuel capacity

$\dot{m}_{max}$ Fuel consumption rate at maximum output

n Order of plant

n_i^* Relative degree of individual elements of $W_p(s)$

p Body roll rate

P Adaptation gain matrix

P_{bhp} Engine brake power

q Body pitch rate

Q Control Matrix

Q_0 Positive definite matrix

r Body yaw rate

r_m Reference input

$r_q(s)$ Hurwitz monic polynomial of degree $\nu - 1$

$R_m(s)$ Polynomial matrix of monic Hurwitz polynomials

$R_p(s)$ Polynomial matrix in coprime matrix fraction decomposition of $W_p(s)$

$R_q(s)$ Diagonal matrix of polynomial transfer functions

R_{FB} Radius of center of flybar paddle

R_{mr} Main rotor radius

$R_{p_{ad}}(s)$ Adjoint of $R_p(s)$

$R_{p_{rc}}$ Matrix column form of $R_p(s)$

R_{tr} Tail rotor radius

s_{FB} Span of flybar paddle

S_a Selector matrix

S_{ld} Selector matrix

S_{li} Selector matrix

T Post-compensator matrix

T_i Nonsingular matrices made of unit vectors $i = 1, 2$

u Forward Velocity (body frame), ft/sec

u_p System input linearized about nominal trim

u_{pe} System input linearized about trim

U System input

U_0 Nominal trim input to plant

U_0^* Searched nominal trim input

U_1 Intermediate nominal trim input during search

U_e Trim input to plant

U_g Forward velocity (ground frame), ft/sec

U_{col} Main rotor collective

U_{pcyc} Main rotor pitch cyclic

U_{ped} Tail rotor collective

U_{rcyc} Main rotor roll cyclic

U_{thr} Engine throttle

v Lateral Velocity (body frame), ft/sec

v_p Input with precompensation

V_w Wind velocity vector (local-level frame)

w Vertical Velocity (body frame), ft/sec

$W_a(s)$ Gradient stabilizer transfer function matrix

$W_c(s)$ Precompensator transfer matrix

W_g Vertical velocity (ground frame), ft/sec

$W_m(s)$ Reference model transfer function matrix

$W_p(s)$ Plant transfer function matrix

$\overline{W}_p(s)$ Plant with precompensator

$W_{cl}(s)$ Closed loop transfer function matrix

x North position (local-level frame), ft

x_m Reference model state

x_p System state linearized about nominal trim

x_{ht} Horizontal tail c.p. location (forward of c.g.)

x_{mr} Main rotor hub location (forward of c.g.)

x_{pe} System state linearized about trim

x_{tr} Tail rotor hub location (forward of c.g.)

x_{vt} Vertical tail c.p. location (forward of c.g.)

X System state

X_0 Nominal trim state of plant

X_0^* Searched nominal trim state

$\dot{X}_0$ Commanded state derivative for nominal trim

$\dot{X}_{0_3}$ Part of nominal trim state derivative

$\dot{X}_{0_4}$ Part of nominal trim state derivative

X_1 Intermediate nominal trim state during search

X_a Fixed part of nominal trim

X_b Part of nominal trim determined through search

X_c Commanded state

$\dot{X}_c$ Commanded state derivative

$\dot{X}_{c_3}$ Part of commanded state derivative

$\dot{X}_{c_4}$ Part of commanded state derivative

X_e Trim state of plant

$\dot{X}_e$ Commanded state derivative for trim

X_g North position (ground frame) ft

X_{0_1} Part of nominal trim state

X_{0_2} Part of nominal trim state

X_{c_1} Part of commanded state

X_{c_2} Part of commanded state

$X_{uu,fus}$ Axial fuselage drag coefficient

Y System output

y East position (local-level frame), ft

y_c Commanded output linearized about nominal trim

y_{pe} System output linearized about trim

Y_c Commanded output

Y_g East position (ground frame) ft

$Y_{uu,vt}$ Trim vertical tail lift coefficient

$Y_{uv,ht}$ Vertical tail lift coefficient due to sideslip angle

$Y_{vv,fus}$ Lateral fuselage drag coefficient

$Y_{vv,ht}$ Vertical tail lift coefficient due to sidewash

$Y_{VV,vt,max}$ Maximum vertical tail lift coefficient

z Down position (local-level frame), ft

z_m Modified reference output

z_p Modified plant output

z_{fus} Fuselate c.p. location (below c.g.)

z_{ht} Horizontal tail c.p. location (below c.g.)

z_{mr} Main rotor hub location (below c.g.)

z_{tr} Tail rotor hub location (below c.g.)

z_{vt} Vertical tail c.p. location (below c.g.)

$Z_c(s)$ Controller polynomial matrix

$Z_d(s)$ Controller polynomial matrix

$Z_p(s)$ Polynomial matrix in coprime matrix fraction decomposition of $W_p(s)$

$Z_{uu,ht}$ Trim horizontal tail lift coefficient

$Z_{uw,ht}$ Horizontal tail lift coefficient due to angle of attack

$Z_{VV,ht,max}$ Maximum horizontal tail lift coefficient

$Z_{ww,fus}$ Vertical fuselage drag coefficient

$Z_{ww,ht}$ Horizontal tail lift coefficient due to downwash

1 Introduction

The control problem of high-performance helicopters is a challenging task since the vehicle dynamics are highly nonlinear and fully-coupled (Figure 1),[1] and subject to parametric uncertainties. Often, during complex maneuvers, the thrust is a function of roll, pitch and heading angles. Control inputs are invariably limited to variations in pitch of main rotor and tail rotor blades and the throttle. In addition, the tail rotor needs to exactly cancel out the rotational torque due to the main rotor in order for the helicopter to maintain steady yaw angle. Some of the system parameters can change with the environment (e.g. the aerodynamic constants) or with the helicopter (e.g. lift curve slopes). The unknown system parameters also cause the trim conditions for the helicopter to be unknown. The complexity of this problem remains just as high in the case of both unmanned helicopters where remote communications with the ground are used for control as well as autonomous

helicopters where it is expected that little or no information from the ground is utilized for control. In this paper, our focus is on the latter for which we develop an adaptive multivariable controller that is capable of simultaneously accommodating all coupling features, parametric uncertainties, and the trim error, and as a result executes complex maneuvers autonomously.

Great strides have been made in unmanned helicopter technology in the past few decades. Controller designs for these vehicles have involved highly augmented controller structures.[2–5] These controllers have multiple-inputs and multiple-outputs, are robust and have enabled aggressive flight performance while ensuring stability. Typically, in such vehicles, remote communications are maintained with a ground station for obtaining ground-based reference signals which are in turn used to compute the desired control inputs. In contrast, in an autonomous helicopter, the controller has to generate the appropriate action without these reference signals and still deliver the requisite high performance. A direct consequence of this is the introduction of an unknown trim error which can be eliminated by a pilot and a ground station in a manned and unmanned helicopter, respectively. This problem is further exacerbated in the context of system uncertainties which introduce an additional unknown component into the trim error as the trim commands change with the uncertainties. While the incorporation of integrals can help mitigate this problem, it is often at the expense of trading off performance. What is more desirable is a control methodology that is capable of adapting to the trim error while simultaneously accommodating all coupling features and parametric uncertainties during the execution of maneuvers.

Previous work on linear control design for helicopters includes the use of Eigenstructure Assignment,[6–8] H_2, H_∞,[9] μ-synthesis,[10,11] and dynamic inversion methods.[12] These methods are based on linearized helicopter models about hover, uniform forward flight trim conditions, or the assumption that the modes are decoupled. Nonlinear control designs previously attempted include neural network based controllers,[13] fuzzy control,[14,15] differential flatness,[16] and backstepping designs.[17] These methods either assume feedback linearizability, which in turn restricts the motion to be around hover, or do not include parametric uncertainties, or realistic aerodynamics. Specific issues such as unknown trim conditions that degrade the performance of the helicopter have not been addressed. While adaptive control schemes have been proposed in the aircraft and spacecraft control context,[18] there is a lack of similar work on helicopter control. The non-minimum phase nature of the helicopter dynamics adds to the challenge of finding a stable adaptive controller.

In this paper, our objective is to present an adaptive controller that addresses the special needs of autonomous vehicles. The proposed multivariable adaptive controller is comprised of the following features: it accommodates both parametric and unknown trim conditions through online adjustments of parameters. Suitable Lyapunov functions insure closed loop stability and robustness. The control design judiciously integrates linear design with online adaptive strategies, so as to maximize benefit from off-line information and on-line measurements. A two-step nonlinear optimization procedure is carried out to determine nominal trim states that allows the arbitrarily close convergence to the global minima by making use of prior information available about sub-components of the trim states during a given maneuver. The performance of the controller is demonstrated using a high fidelity nonlinear simulation model of Draper Laboratory's autonomous helicopter.

The new control design structure, together with a trim error estimate, controller parameter update laws and system augmentation for stable adaptation leads to a stable robust system with enhanced performance, thereby resulting in a viable multivariable adaptive controller for helicopters. Overall, the suggested design methodology reduces the gap between state of the art adaptive control theory and design for non-full-state feedback systems and the needs of realistic applications such as autonomous helicopters.

The paper is organized as follows. In section 2 the problem is stated and a brief description of the nonlinear model of the helicopter dynamics used in section 3 is presented. In section 3 the adaptive control design methodology is presented. Section 4 compares the performance of the adaptive controller with that of other controllers using different scenarios, while Section 5 offers conclusions.

2 Statement of the Problem

In this section, a statement of the problem and the helicopter model used for the design of the adaptive controller is described in Section 2.1. The unknown trim conditions are described in Section 2.2 and the effect of using a nominal trim is described in Section 2.3.

2.1 The Control Problem

Our goal is to design controllers for autonomous helicopters so that accurate command following is achieved. A helicopter dynamics model developed at Draper Laboratory,[1,19–21] is used to develop the control design. This model is obtained by considering the fuselage of the helicopter as a rigid body attached to the main rotor and tail rotor. The 6-DOF equations of the fuselage are derived from Newton's second law.

The system can be expressed as an equivalent block, f, in the following manner.

$$\dot{X} = f\left(X, U, \Theta\right), \tag{1}$$

For the helicopter,

$$X = [e_0, e_1, e_2, e_3, u, v, w, p, q, r, x, y, z, \Omega, a_1, b_1, a_{1,FB}, b_{1,FB}, \lambda_f]^T, \tag{2}$$

$$U = [U_{rcyc}, U_{pcyc}, U_{ped}, U_{col}, U_{thr}]^T, \tag{3}$$

$$\begin{aligned}\Theta = [&m_e, m_f, g, I_{xx}, I_{yy}, I_{zz}, x_{mr}, z_{mr}, R_{mr}, a_{mr}, b_{mr}, c_{mr}, C_{D0,mr},\\ &I_b, K_{GE}, R_{FB}, a_{FB}, c_{FB}, s_{FB}, I_{FB}, K_{cyc}^{FB}, K_{FB}^{cyc}, \rho, x_{tr}, z_{tr},\\ &D_{tr}, R_{tr}, a_{tr}, b_{tr}, c_{tr}, C_{D0,tr}, P_{bhp}, \eta, \Omega_{max}, \dot{m}_{max}, D_e, z_{fus},\\ &X_{uu,fus}, Y_{vv,fus}, Z_{ww,fus}, x_{ht}, z_{ht}, Z_{uu,ht}, Z_{uw,ht}, Z_{ww,ht},\\ &Z_{VV,ht,max}, x_{vt}, z_{vt}, Y_{uu,vt}, Y_{uv,vt}, Y_{vv,vt}, Y_{VV,vt,max}].\end{aligned} \tag{4}$$

Of the state variables in X, $a_1, b_1, a_{1,FB}, b_{1,FB}$, and λ_f are difficult and expensive to measure and are therefore not available in most cases. Similarly, an exact measure of λ_f is also usually not available. Therefore, the system output is given by

$$Y = [e_0, e_1, e_2, e_3, u, v, w, p, q, r, x, y, z, \Omega]. \tag{5}$$

In terms of the vehicle model described in Equations (1)–(5) the problem under consideration can therefore be stated as follows. For the system given by Equations (1)–(5), the objective is to find U such that $Y \rightarrow Y_c$ while all other signals remain bounded in the presence of uncertainties in the helicopter and environment, for any given operating condition.

2.2 Effect of Unknown Trim Conditions

One of the most common methods of controlling the nonlinear system in (1) is through linearization. The linearized model corresponding to (1) is given by

$$\dot{x}_{pe} \;=\; Ax_{pe} + Bu_{pe} \qquad y_{pe} = Cx \tag{6}$$

where

$$x_{pe} \;=\; X - X_e, \qquad u_{pe} \;=\; U - U_e, \qquad y_{pe} = Y - CX_e. \tag{7}$$

Suppose the goal is to carry out a forward flight or a vertical climb. X_e, U_e must satisfy the equation

$$f(X_e, U_e, \Theta) = 0 \tag{8}$$

The determination of trim conditions for a given maneuver is tantamount to finding solutions of a set of nonlinear equations as in (8). This determination becomes even more complex in the presence of uncertainties. This is because of the fact that Θ in (8) is unknown and therefore the trim conditions X_e, U_e which are obtained as solutions of (8) are unknown as well. As a result, x_{pe}, u_{pe}, and y_{pe} in Eq. (7) are not measurable. Therefore even the very first step in the control design cannot be taken due to the presence of uncertainties.

One possible approach for overcoming this difficulty is to estimate Θ at a simple maneuver, such as the hover, using parameter identification methods, and proceed to determine X_e, U_e and therefore the linear controller using (6). However, as environmental and system conditions change during the vehicle maneuvers, new changes in Θ can occur. These in turn necessitate continued estimation of either Θ, or its effects on the trim conditions. We adopt such an approach in this paper of an adaptive control design where the unknown trim condition is estimated on-line in addition to the estimation of the control parameters, to generate the desired control input.

2.3 Nominal Trim Condition

Since pilot action to achieve the trim conditions in flight, $X_e(\Theta), U_e(\Theta)$, is not available in the case of an autonomous helicopter, we choose a pseudo-trim condition, X_0, U_0, for a known nominal

value, Θ_0, of Θ. Thus,

$$X_0 = X_e(\Theta_0), \tag{9}$$

$$U_0 = U_e(\Theta_0). \tag{10}$$

Linearizing the plant in equation (1) about X_0, U_0, for simple maneuvers that satisfy (8) we obtain that

$$\begin{aligned} \dot{x}_p &= A_p(\Theta)\, x_p + B_p(\Theta)\, u_p + d_x(\Theta), \\ y_p &= C x_p + d_y(\Theta), \end{aligned} \tag{11}$$

$$\begin{aligned} d_x(\Theta) &= A_p(\Theta)(X_0 - X_e) + B_p(\Theta)(U_0 - U_e), \\ d_y(\Theta) &= C(X_0 - X_e). \end{aligned} \tag{12}$$

where $x_p = X - X_0$, $u_p = U - U_0$ and $\dot{x}_p = \dot{X} - \dot{X}_0$. It can be seen from this equation that an unknown constant disturbances $d_x(\Theta), d_y(\Theta)$ is now added because of the unknown trim conditions. The matrices $A_p(\Theta), B_p(\Theta)$ are also affected by parametric uncertainties. An adaptive controller, to accommodate the parametric uncertainties and compensate for the unknown trim, is therefore considered for control of this system. The objective is to design a u_p such that y_p follows y_c where

$$y_c = Y_c - C X_0. \tag{13}$$

The above problem statement becomes more complex in the context of a complex maneuver. In such a case, unlike (8), given X_c, X_0, U_0 satisfy the equation

$$f(X_e, U_e, \Theta) = \dot{X}_c \tag{14}$$

where, $\dot{X}_c$ is not only nonzero but only partially specified. For example, in a coordinated turn, for a specified u and $\dot{\Psi}$, p is known to be zero, but ϕ is to be determined; θ is zero (or a small value) but q needs to be calculated. In such cases, the solutions X_e and U_e need to be found using the following procedure: Let

$$X_0 = T_1 \begin{bmatrix} X_{0_1} \\ X_{0_2} \end{bmatrix}, \qquad \dot{X}_0 = T_2 \begin{bmatrix} \dot{X}_{0_3} \\ \dot{X}_{0_4} \end{bmatrix}, \qquad X_c = T_1 \begin{bmatrix} X_{c_1} \\ X_{c_2} \end{bmatrix}, \qquad \dot{X}_c = T_2 \begin{bmatrix} \dot{X}_{c_3} \\ \dot{X}_{c_4} \end{bmatrix} \tag{15}$$

$$X_{0_1} = X_{c_1}, \qquad \dot{X}_{0_3} = \dot{X}_{c_3}. \tag{16}$$

X_{c_1} and $\dot{X}_{c_3}$ are specified by the maneuver. X_0, $\dot{X}_0$ and U_0 can now be calculated using (7), (8) and (15). Linearizing the plant as before about X_0, U_0 we obtain the same plant description as in (11) but with $d_x(\Theta)$ given by

$$d_x(\Theta) = A_p(\Theta)(X_0 - X_e) + B_p(\Theta)(U_0 - U_e) + \dot{X}_e - \dot{X}_0 \tag{17}$$

and $d_y(\Theta)$ as in (12).

3 Adaptive Control Design

The problem that we address in this section is the control of the plant in (11) where A_p, B_p, d_x, and d_y are unknown, such that y_p follows y_c defined in equation (13). The plant can be represented in an input-output form given by

$$y_p = W_p(s)[u_p + d_0] + d_1 \tag{18}$$

where

$$W_p(s) = C(sI - A(\Theta))^{-1} B(\Theta) \in \mathbb{R}_p^{m \times m}(s). \tag{19}$$

d_0 is the effective input disturbance and is, therefore, canceled out using a trim error estimate added to u_p.

In section 3.1 the controller structure is described after which the specific components required for its implementation on the helicopter are described in section 3.2. The adaptive control laws are described in section 3.3.

3.1 Controller Structure

We use a model-reference approach to determine the adaptive rules for adjusting the controllers. This requires the choice of a reference model specified by the input-output relation

$$y_m = W_m(s) r_m. \tag{20}$$

One convenient and simple choice of the transfer function matrix $W_m(s)$ is given by

$$W_m(s) = R_m(s)^{-1} \tag{21}$$

where $R_m(s)$ is a polynomial matrix whose entries are monic Hurwitz polynomials. The controller structure can be described as follows:[23]

$$\begin{aligned} u_p &= \Theta_c \omega(t), \\ \omega &= \left[r_m, \omega_1^T, ..., \omega_{\nu-1}^T, \omega_\nu^T, ..., \omega_{2\nu-1}^T\right]^T, \\ \Theta_c &= [K_0, C_1, ..., C_{\nu-1}, D_0, ..., D_{\nu-1}], \\ \omega_i(t) &= \frac{s^{i-1}}{r_q(s)} u(t), \quad i = 1, ..., \nu-1, \\ \omega_j(t) &= \frac{s^{j-\nu}}{r_q(s)} y_p(t), \quad j = \nu, ..., 2\nu-1 \end{aligned} \tag{22}$$

C_i and D_j are chosen such that the closed-loop system has poles at desired locations. The well-known Bezout Identity can be used to be determine the appropriate values of C_i and D_j, as follows:

$$[(R_q - Z_c) R_p - Z_d Z_p] = R_q K_0 W_m^{-1} Z_p, \tag{23}$$

$$W_p(s) = Z_p(s) R_p^{-1}(s), \tag{24}$$

$$\begin{aligned} R_q(s) &= \mathrm{diag}\left(\frac{1}{r_q(s)}\right), \\ Z_c(s) &= \textstyle\sum_{i=1}^{\nu-1} C_i s^{i-1}, \\ Z_d(s) &= \textstyle\sum_{j=0}^{\nu-1} D_j s^j. \end{aligned} \tag{25}$$

where $Z_p(s)$ and $R_p(s)$ are in right coprime form. For the closed-loop transfer function matrix to match $W_m(s)$, we need (a) K_0 to be nonsingular, and (b) $Z_p(s)$ to be stably invertible. For known values Θ, the pole-placement controller is completely specified by the equations (22)–(25). It should be noted that in many applications, the plant description is not readily available in the form of coprime matrices.

3.2 Pole Placement Control Design

As mentioned in the introduction, the dynamic model of autonomous helicopters is given by equations (1)–(5). These equations can then be linearized as in (11) where the nominal trim values X_0 and U_0 are to be computed for each maneuver. The controller for the plant in (11) is specified by equations (22), (25), and (23). The complete control design requires the following steps to be executed: (1) Determine the nominal trim conditions X_0 and U_0 which are the solutions of (8) when $\Theta = \Theta_0$. (2) Determine the coprime matrices Z_p and R_p from the linearized plant parameters $A_p(\Theta_0)$, $B_p(\Theta_0)$, and C. (3) Ensure that the high frequency gain K_p is nonsingular. (4) Ensure that

the matrix Z_p is stably invertible. The details of steps 1-4 are given in sections 3.2.1 through 3.2.4, respectively. An additional property of the relative degree of the plant model of a helicopter is outlined in section 3.2.5 which leads to a simple adaptive control design.

3.2.1 Determination of Nominal Trim Values X_0, U_0

In order to find the trim conditions X_0 and U_0 that are the solutions of (8), 19 highly coupled nonlinear equations have to be solved, and hence an explicit determination of the solutions X_0 and U_0 is near impossible. Optimization schemes need to be used to find a solution to this equation. Linear methods like Simplex are seen to converge to a local minima from almost all starting values. Nonlinear methods such as Simulated Annealing or Genetic Algorithms are computationally expensive. A simpler way of solving this problem is now presented which exploits insight into the nature of the helicopter dynamics and consists of a two stage optimization procedure for accurate trim determination.

Often a part of the overall state that includes the attitude angles and angular rates have, either, a small value for most maneuvers, or values that can be determined reasonably accurately. Defining $X_a = [\phi, \theta, \psi, p, q, r]^T$, we fix $X_a = X_{ac}$, and use a simplex search to determine the remaining component X_b of X_0 and U_0. Denoting the resulting values X_1 and U_1 that this simplex search leads to, in the second stage of the nonlinear optimization, we begin with X_1 and U_1, and carry out a simplex search in the overall (X, U) space to result in the final trim determination of (X_0^*, U_0^*).

The above two-step procedure has the potential to converge to the global minimum mainly because of the prior information available about the trim values of a sub-component of the state variables and inputs. This information is most likely available even in the most complex maneuvers, and therefore the above procedure is a valuable step in the control design.

3.2.2 Coprime Matrix Fraction Decomposition

The next step in the control design is to find coprime matrices, $Z_p(s)$ and $R_p(s)$, starting from time-domain matrices A_p, B_p, and C, as in equations (11). Diagonalizing the numerator matrix of $W_p(s)$ and separating out the poles from the transmission zeros is very sensitive to numerical errors. For the helicopter, therefore, the algorithm suggested in Bigulac and Vanlandingham[25] for

right coprime matrix fraction decomposition is used. The algorithm is briefly outlined below.

1. Form Selector matrices S_a, S_{ld}, S_{li} using pseudo-controllability indices.

2. With $A_c(\Theta)$, the controllable canonical form of $A_p(\Theta)$, get $R_{p_{rc}}$, using the equations

$$R_{p_{rc}} = S_{ld} - S_{li} A_c S_a. \tag{26}$$

3. Find $Z_p(s)$ using the following equations

$$N(s) = Z_p(s) R_{p_{ad}}(s), \tag{27}$$

$$\sum_{j=0}^{i} Z_{p_j} R_{p_{ad_{i-j}}} = N_i, \quad i = 1, ..., n. \tag{28}$$

This algorithm is found to give a reasonably accurate representation $Z_p(s)$ and $R_p(s)$.

3.2.3 Non-singular High Frequency Gain

The next step is to find $Z_c(s)$ and $Z_d(s)$, using $Z_p(s)$ and $R_p(s)$, and equation (23). We note that a necessary requirement for finding $Z_c(s)$ and $Z_d(s)$ is the nonsingularity of K_p. In the case of the helicopter, the relative degree of some columns of $W_p(s)$ is higher than others. That is, there are some elements of the input vector u which have lower relative degree transfer functions to all outputs when compared to the other transfer functions. This results in the high frequency gain matrix K_p to have the columns corresponding to these input elements to be identically zero. Therefore, K_p is not invertible. This problem can be resolved by filtering these input elements through stable filters of appropriate degree. A pre-compensator of the form

$$W_c(s) = diag\frac{1}{\pi_p^{k_i}}, \tag{29}$$

is selected, where k_i are equal to the maximum of the minimum column relative degree of the matrix minus the minimum column relative degree of the column i. The new input to the system v_p is given by

$$v_p = W_c(s) u_p. \tag{30}$$

This changes the new transfer function of the plant to the following:

$$\overline{W}_p(s) = W_p(s) W_c(s). \tag{31}$$

We note that $\overline{W}_p(s)$ has a high frequency gain $\overline{K}_p$ which is obviously different from K_p, and nonsingular. This enables us to find $\overline{K}_0 = \overline{K}_p^{-1}$ in the Bezout Identity equation (23) corresponding to $\overline{W}_p(s)$. $\overline{K}_0$ is also non-singular which is needed for stable adaptation.

3.2.4 Minimum Phase Plant

In order to solve (23) without unstable pole-zero cancellations, we need the transmission zeros, i.e. the roots of $\det Z_p(s)$ to be stable. This implies that $Z_p(s) R_p^{-1}(s)$ is minimum phase. With the input U as in (3) and output Y as in (5), we proceed to design an output $z(t) \in \mathbb{R}^5$ such that

$$z_p(t) = T y_p(t). \tag{32}$$

where T is a post-compensator chosen such that $TZ_p(s)$ is square and has stable transmission zeros over the entire range of parameter space of interest. One natural choice of such a z_p is $z_p = [p, q, r, w, \Omega]^T$ added to other states available in (5) such that $\det Z_p(s)$ is stable. This gives us a nearly decoupled system with stable transmission zeros and no unstable pole-zero cancellations.

3.2.5 Helicopter Relative Degree

For the helicopter model, it is seen that the relative degree n_i^* of the individual elements of $W_p(s)$ is 1 or 2. This is because the relative degree of the transfer function from the thrust force to the velocity is 1 from Newton's second law. The thrust forces in turn are dependent upon the angular displacement of the rotor blades. These angular displacements a_1 and b_1 are described by a relative degree 1 transfer function from the inputs U_{pcyc}, U_{rcyc}.

If the relative degree n_i^* is unity the adaptive controller requires $m \times (2m\nu + 1)$ controller parameters, and $2m\nu$ states as can be seen in equations (22) since the notion of a strictly positive real transfer function can be exploited. A slight extension to the same controller structure suffices for the case when n_i^* is equal to two,[26] which requires no additional parameters but an additional filtered output of ω. The number of states and parameters in both cases are significantly smaller than those in the case when n_i^* is greater than two. For a plant with $m = 5$ and $\nu = 4$, the controller states are 80 when $n_i^* = 2$ in comparison to 440 when $n_i^* = 3$.

The complete system is now represented by the following equation:

$$z_p = TZ_p(s) R_p^{-1}(s) W_c(s) (u_p + d_0(\Theta)) + T d_1(\Theta). \tag{33}$$

Here $Z_p(s) R_p^{-1}(s)$ is the coprime matrix fraction decomposition of the state space model in equation (11). The output in equation (5) is assumed to have all available states.

3.3 Adaptive Pole-Placement Control

The adaptive controller is now designed for the partial state feedback case of the helicopter. The system is described by equations (11), and with the addition of the precompensator and post-compensator, the transfer function changes to the representation in equation (33). An adaptive controller structure based on the structure in pole-placement controller described before is now chosen for the helicopter. In order to compensate for d_0 in (18), ω and Θ_c are augmented as $\bar{\omega} = \left[\omega_0^T, \omega^T\right]^T$, and $\bar{\Theta}_c(t) = \left[\hat{d}^T(t), \Theta_c^T(t)\right]^T$ which results in the controller

$$u_p(t) = \bar{\Theta}_c(t)\bar{\omega}(t). \tag{34}$$

We define $\bar{\Theta}_c^*$ as the constant value of the controller parameters for which the closed loop transfer function satisfies $W_{cl}(s) \equiv H_p(s)$. $H_p(s)$ is the hermite normal form of the plant in equation (33) and is diagonal.[26] The error, $e_1(t) = z_p(t) - z_m(t)$, is derived as

$$e_1(t) = H_p(s) K_p \Phi(t) \bar{\omega}(t) + T d_1(\Theta). \tag{35}$$

where $\Phi(t) = \bar{\Theta}_c(t) - \bar{\Theta}_c^*$ and z_m is the output of the reference plant

$$z_m(s) = H_p(s) r_m. \tag{36}$$

For stable adaptation the transfer function $H_p(s)$ needs to be Strictly Positive Real (SPR). If the elements of $H_p(s)$ are of relative degree 2 the input and error equations are modified as

$$u(t) = \dot{\overline{\Theta}}_c(t) W_a(s) \overline{\omega}(t) + \overline{\Theta}_c(t) \overline{\omega}(t), \tag{37}$$

$$e_1(t) = H_p(s) W_a^{-1}(s) K_p \Phi(t) \omega(t) + T d_1(\Theta), \tag{38}$$

where

$$W_a(s) = \frac{1}{s+a} I \quad a > 0 \tag{39}$$

and chosen such that $H_p(s)W_a(s)$ is SPR.[26] The following adaptation law is now chosen for chosen for stable adaptation:

$$\dot{\overline{\Theta}}_c = -Pe_1 W_a(s)\bar{\omega}^T - \Gamma_r \overline{\Theta}_c, \quad \Gamma_r > 0 \tag{40}$$

$$P = \Gamma^{-1} \tag{41}$$

where

$$\Gamma K_p + K_p^T \Gamma = Q_0 > 0, \quad \forall \Theta \in \Theta_s. \tag{42}$$

Γ_r is chosen for robustness of the design to the trim disturbance $d_1(\Theta)$, nonlinearities, noise, and other disturbances.

The initial value of K_0 is the inverse of K_p^{-1}, for the plant in equation (33) with nominal values for Θ. The initial value of $\hat{d}$ is chosen as zero. The initial values of the rest of the controller parameters Θ_c are found by solving (23) with W_m replaced by H_p, i.e., by solving

$$[(R_q - Z_c)R_p - Z_d Z_p] = R_q K_0 H_p^{-1} Z_p. \tag{43}$$

Theorem 4.1 *For the plant given in equation (33), model in equation (36), and controller given in equation (37), given a $H_p(s)W_a(s)$ that is strictly positive real, and a K_p which satisfies equation (42), the adaptation law in equation (40)–(41) guarantees that all signals of the closed loop system are bounded.*

The reader is referred to Narendra and Annaswamy[26] for the proof.

4 Numerical Studies

The controller presented in the previous section is simulated for the nonlinear dynamics presented in section 2.1. 2% and 20% increases in m and I_{yy} are used as the uncertainties. These parameters are seen to have the worst impact on the stability of the system and an increase in their values is seen to have the most effect. Four different tasks are performed and the results of the dynamic inversion controllers are compared against the adaptive controller. Adaptation is stopped after a time in each case based on the output error value to observe learning behavior of the controller. The results can be summarized in Table 1.

The simulations use a high-fidelity model of the helicopter including aerodynamics and thrust calculations as described in Johnson et al.[21] However, for tasks 1 and 2 the model is simplified to only the longitudinal dynamics and with the actuator dynamics neglected. The complete model with actuator dynamics is used for tasks 3 and 4. Since this study represents a first step in the design of a truly autonomous helicopter, the saturation constraints on the inputs have not been incorporated. The proposed controller is demonstrated in comparison with other existing controllers designed with the same assumptions.

4.1 Controllers for Comparison

We use three fixed controllers based on linear LQ method,[9] dynamic inversion (DI),[12] and integrator based design,[9] whose performances will be compared to the adaptive controller presented in this paper.

4.2 Task 1: Track Step Changes in Forward Flight Velocity

The first simulation involves step changes in forward flight velocity between $28 ft/sec$ and $40 ft/sec$* for the helicopter. In this maneuver, random steps are taken subsequent to the stoppage of adaptation to test the learned behavior of the adaptive controller. The LQ–controller, designed without the inclusion of aerodynamics, and assuming full state access, is compared against the adaptive controller. Since in this case, all relevant states are accessible, a simpler adaptive controller of the form

$$u_p = Q\left(Kx_p + r_m + \hat{d}\right), \tag{44}$$

$$\dot{K} = -\Gamma_1\left[B_m^T P e x_p^T + \Gamma_{r1} K\right], \tag{45}$$

$$\dot{Q} = -\Gamma_2\left[Q B_m^T P e {u_p}^T Q - \Gamma_{r2} Q\right], \tag{46}$$

$$\dot{\hat{d}} = -\Gamma_3\left[B_m^T P e + \Gamma_{r3}\hat{d}\right], \tag{47}$$

was used, whose details can be found in Krupadanam.[22] The LQ-controller has the same structure as in Eq. (44) where Q and K are fixed at values that minimize a suitable quadratic cost function

*Higher speeds can be achieved with this controller by gain-scheduling. We also note that tasks 3 and 4 address more complex maneuvers where gain-scheduling was used successfully. For ease of exposition, the speed was limited to $40 ft/sec$ It should be noted that this speed is significantly larger than what was previously studied in the Draper simulation studies[21]

and $\hat{d}$ set to zero.

Figure 3 compares the adaptive controller against the LQ–controller with aerodynamics included in the system design. It can be seen that the LQ–controller has a large steady state bias. This is because the nonlinear part of the dynamics due to the aerodynamics are neglected in the design. The response of a reference model are also included in figure 3 where the reference model corresponds to the nominal linearized dynamics of the plant with the LQ–controller. The adaptive controller was chosen as in equations (44)–(47), but with $\hat{d}$ fixed as zero, and with the starting values for K and Q as those for the LQ–controller. As shown in figure 3, the steady-state bias is reduced by as much as 95% in the adaptive case. As shown in figure 3, even though adaptation was stopped at 320 seconds, the adaptive controller continues to outperform the LQ–controller.

In order to address the issue of steady state bias an integral action was added to the DI–controller, and the $\hat{d}$ term was adjusted as in equation (47) of the adaptive controller. The resulting response is shown in figure 4. Dynamic inversion reduces the steady state bias compared to the LQ–controller. The addition of integrators eliminates steady state error but increases transients for the dynamic inversion controller. For example, for a control design which maintains a rise time of less than 5 seconds, transients of magnitude upto 10% of the step size and settling time greater than 40 seconds are introduced with integral action. In contrast, the adaptive controller is seen to outperform this controller by having low steady state bias, fast rise time and no overshoot or transients after the initial adaptation. The initial transients introduced by the adaptation are of similar magnitude as those of the DI–controller with integrators. These are eliminated in subsequent iterations of the maneuver as the controller parameter errors decrease. Finally, even after the adaptation is stopped, the controlled system continues to show the learned performance.

Figure 5 shows training of the adaptive controller for a series of steps followed by stoppage of adaptation. Random steps are then taken in forward velocity with the same controller values. This shows that the controller gains and trim error estimate learned in the initial series of constant steps is sufficient to provide good performance for maneuvers of similar frequency content. This is because the adaptation enables the controller to minimize the state error for the particular maneuver. The controller gains are therefore values that make the adapted system similar to the reference model for these frequencies.

The main rotor pitch flapping angle, a_1, is shown in figure 6 for the first 180 seconds which

correspond to three initial steps in forward veloicty. It is seen that the bandwidth requirements are similar for the adaptive and DI–controller in the first two steps. The maximum required magnitude and angular rates for a_1 are around 7 and 65 seconds for the DI–controller and adaptive controller respectively. From the third step onwards the bandwidth requirements are lower for both cases as seen from the transients. The maximum main rotor flapping angular rate is less than $10^0/sec$ for both the adaptive and DI-controller. Thus the adaptive controller achieves better performance in the long run without any greater bandwidth requirements on the inputs.

4.3 Task 2: Complex Maneuver in Forward and Vertical Velocities

We now a consider a maneuver that is to jump over hurdles, i.e., to track a circle in the $U_g - W_g$ plane. Since the commanded velocities vary significantly, a gain-scheduled approach is used with 12 distinct operating points along the maneuver, both for the adaptive and the DI–controller. The DI controller is designed as in task 1, with integrators. The adaptive controller as in equations (44)–(47) in task 1 is used. The resulting performances are shown in figures 7 and 8. The DI–controller is seen to have very large initial transients, and with time, the integral action reduces the tracking error. In contrast, the adaptive controller results in smaller transients (see Figure 7) and in an even smaller tracking error (see Figure 8).

4.4 Task 3: Vertical Flight with Partial State Access

The controller presented in the section 3 is now simulated for the full helicopter dynamics presented in section 2.1 with a 20% uncertainty in the mass. The task performed involves steps in vertical velocity that varies between 5 ft/sec and 10 ft/sec. The resulting sysem has four inputs and four outputs with the throttle kept constant. The states that are not accessible are $a_1, b_1, a_{1,FB}, b_{1,FB}$ and λ_f. The results of the adaptive controller are compared with a pole-placement controller of a similar structure but with fixed parameters which are 96 in number. Adaptation is stopped in the former case, after a certain time as in tasks 1 and 2, to observe learning. It needs to be noted that, the adaptive controller design includes, as initial values for the control parameters, plant parameters obtained with linearization around nominal parameter values with the aerodynamics included. At these speeds a design that neglects aerodynamics has inadequate robustness properties and invariably, simulations fail because of unacceptably large transients.

The resulting performances of the controllers in the states w and u are shown in Figures 9, 10, which illustrate that the adaptive controller outperforms the pole-placement controller in terms of steady state error and transients. In the case of the forward velocity, the transients are seen to be lower than the pole-placement controller. The figures also show that the adaptive controller exhibits a suitable learning behavior; even though the adaptation is switched off after just two cycles, the tracking performance is seen to be as good as in the last adaptive cycle. The adaptive controller also eliminates the steady state bias.

4.5 Task 4: Coordinated Turn

In this maneuver, the helicopter moves from a coordinated turn of $2.5^\circ/sec$ to $5^\circ/sec$ with a forward velocity of $5ft/sec$. A 20% uncertainty in the mass is added to the system. The requisite controller in this case has 200 parameters. As in task 4, we compare the performance of the adaptive controller with a pole-placement controller of a similar structure. In this case too, the adaptive controller is seen to outperform the pole-placement controller (see Figure 11). In this maneuver, over a period of 30 seconds the linear controller is seen to result in a 6.5 feet error in the displacement of the helicopter from the nominal designed model. The helicopter travels about 45 feet in the X_g-direction during this period. The adaptive controller reduces the error to less than 3 feet in the first cycle and to around 2 feet in the second cycle. In addition to the reduction in the steady state error, the transients are reduced with time. Moreover, after stoppage of adaptation, it was observed the learned values of controller parameters continue to show good performance for the maneuver (see Figure 12).

5 Conclusions

This paper provides a design procedure for the multivariable adaptive control of an autonomous helicopter. In the design model, all typically present aerodynamics, parametric uncertainties, and trim error are included. The adaptive controller includes a trim error estimate and provides for stable adaptation even in the presence of non-minimum phase helicopter dynamics. The controllers are demonstrated through simulations for the control of an autonomous helicopter for maneuvers involving trajectory tracking, steady state bias and complex maneuvers and show considerable

improvement with adaptation. The adaptive controller is stable, robust and shows significant improvement in performance over other control designs. This new methodology is a control design tool that helps bridge the gap between multivariable adaptive control theory and the needs of realistic applications such as autonomous helicopters.

6 Acknowledgements

This work was sponsored by Draper Laboratory University Research and Development Grant No. 902. The authors would like to thank the associate editor, Steve Osder, and the anonymous reviewers for their comments and suggestions which helped place the contributions of the paper in proper perspective.

References

[1] Prouty, R. W., "Helicopter, Performance, Stability, and Control," Robert E. Krieger Publishing Company, Malabar,Florida, 1990.

[2] Tischler, M. B., "Assessment of Digital Flight-Control Technology for Advanced Combat Rotorcraft," *Journal of the American Helicopter Society*, vol. 34, No. 4, 1989.

[3] Tischler, M. B., Fletcher, J. W., Morris, P. M., and Tucker, G. E., "Flying Quality Analysis and Flight Evaluation of a Highly Augmented Combat Rotorcraft," *AIAA Journal of Guidance, Control and Dynamics*, vol. 14, No. 5, Sep. – Oct. 1991.

[4] Osder, S., and Caldwell, D., "Design and Robustness Issues for Highly Augmented Helicopter Controls," *AIAA Journal of Guidance, Control and Dynamics*, vol. 15, No. 6, Nov. – Dec. 1992.

[5] Postlethwaite, I., Smerlas, A., Walker, D. J., Gubbels, A. W., Baillie, S. W., Strange, M. E., and Howitt, J., "H_∞ Control of the NRC Bell 205 Fly-by-Wire Helicopter," *Journal of the American Helicopter Society*, vol. 44, No. 4, 1999.

[6] Ekblad, M., "Reduced-Order Modeling and Controller Design for a High-Performance Helicopter," *AIAA Journal of Guidance, Control and Dynamics*, vol. 13, No. 3, pp. 439–449, May – Jun. 1990.

[7] Hess, R. A., and Gorder, P. J., "Quantitative Feedback Theory Applied to the Design of a Rotorcraft Flight Control System," *AIAA Journal of Guidance, Control and Dynamics*, vol. 16, No. 4, pp. 748–753, Jul. – Aug. 1993.

[8] Low, E., and Garrard, W. L., "Design of flight control systems to meet rotorcraft handling qualities specifications," *AIAA Journal of Guidance, Control and Dynamics*, vol. 16, No. 1, pp. 69–78, Jan. – Feb. 1993.

[9] Shim, D. H., Koo, T. J., Hoffmann, F., and Sastry, S., "A comprehensive study of control design for an autonomous helicopter," *37th IEEE Conference on Decision and Control*, 1998.

[10] Dudgeon, G. J. W., and Gribble, J. J., "Helicopter Attitude Command Attitude Hold Using Individual Channel Analysis and Design," *AIAA Journal of Guidance, Control and Dynamics*, vol. 20, No. 5, pp. 962–971, Sep.–Oct. 1997.

[11] Rozak, J. N., and Ray, A., "Robust Multivariable Control of Rotorcraft in Forward Flight: Impact of Bandwidth on Fatigue Life," *Journal of the American Helicopter Society*, vol. 43, No. 7, pp. 195–201, July 1998.

[12] Snell, S. A., and Stout, P. W., "Robust Longitudinal Control Design Using Dynamic Inversion and Quantitative Feedback Theory," *AIAA Journal of Guidance, Control and Dynamics*, vol. 20, No. 5, pp. 933–940, Sep. – Oct. 1997.

[13] Prasad, J. V. R., Calise, A. J., Corban, J. E., and Pei, Y., "Adaptive nonlinear controller synthesis and flight test evaluation on an unmanned helicopter," *IEEE Conference on Control Applications*, 1999.

[14] Sanders, C. P., DeBitetto, P. A., Feron, E., Vuong, H. F., and Leveson, N., "Hierarchical control of small autonomous helicopters," *37th IEEE Conference on Decision and Control*, 1998.

[15] Frazzoli, E., Dahleh, M. A., and Feron, E., "Robust hybrid control for autonomnous vehicle motion planning," *IEEE Transactions on Automatic Control*, 2000.

[16] Koo, T. J., and Sastry, S., "Differential Flatness Based Full Authority Helicopter Control Design," *IEEE Conference on Decision and Control*, 1999.

[17] Frazzoli, E., Dahleh, M. A., and Feron, E., "Trajectory tracking control design for autonomous helicopters using a backstepping algorithm," *American Control Conference*, Chicago, IL, 2000.

[18] Junkins, J. L., and Akella, M. R., "Nonlinear Adaptive Control of Spacecraft Maneuvers," *AIAA Journal of Guidance, Control and Dynamics*, vol. 20, No. 6, pp. 1104–1110, Nov. – Dec. 1997.

[19] Stepniewsky, W. Z., and Keys, C. N., "Rotary-Wing Aerodynamics," Dover Publications, Inc. 1984

[20] Heffley, R. K., and Mnich, M. A., "Minimum-complexity helicopter simulation math model," NASA CR–177476, NASA Ames Research Center, Moffett Field, CA, 1988.

[21] Johnson, E. N., and DeBitetto, P. A., "Modeling and Simulation for Small Autonomous Helicopter Development," *Proceedings of the AIAA Modeling & Simulation Technologies Conference, 1997.*

[22] Krupadanam, A. S., "A Viable Multivariable Adaptive Controller with Application to Autonomous Helicopters," Ph.D. Thesis. Massachusetts Institute of Technology, 2001.

[23] Singh, R. P., "Stable Multivariable Adaptive Control Systems," Ph.D. Thesis. Yale University, 1985.

[24] Anderson, B. D. O., "Multivariable adaptive identification," Technical Report EE7402, University of Newcastle, Australia, 1974.

[25] Bigulac, S., and Vanlandingham, H. F., "Algorithms for Computer-Aided Design of Multivariable Control Systems," Marcel Dekker, Inc., 1993.

[26] Narendra, K. S., and Annaswamy, A. M., "Stable Adaptive Systems," Prentice-Hall, Inc., Englewood Cliffs, N.J., 1989.

List of Tables

1 Summary of numerical simulation tasks. 1

List of Figures

1 Schematic of helicopter dynamics 2

2 The multivariable plant with the proposed adaptive controller 3

3 Comparison of the adaptive and the linear LQ-controller in task 1, step changes in forward flight velocity. The resulting responses of u versus time are shown from 0 to 500 seconds, with adaptation stopped at 320s. The adaptive controller is chosen as in equations (44)–(46) but with no trim estimate. 4

4 Comparison of the adaptive and the linear DI-controller in task 1, step changes in forward flight velocity. The resulting responses of u versus time are shown from 0 to 500 seconds, with adaptation stopped at 400s. The adaptive controller is chosen as in equations (44)–(47) with the trim estimate $\hat{d}$. The DI controller includes an integrating action. 5

5 Comparison of the adaptive and the linear DI-controller in task 1, for random step changes in forward flight velocity after a certain time. The resulting responses of u versus time are shown from 0 to 1200 seconds, with adaptation stopped at 600s. The adaptive controller is chosen as in equations (44)–(47) with the trim estimate $\hat{d}$. The DI controller includes an integrating action. 6

6 Comparison of the adaptive and the linear DI-controller in task 1, for step changes in forward flight velocity. The corresponding control input, a_1, which is the main rotor pitch flapping is shown versus time for the two controllers from 0 to 180 seconds, which corresponds to the first three cycles. The adaptive controller is chosen as in equations (44)–(47) with the trim estimate $\hat{d}$. The DI controller includes an integrating action. 7

7 Comparison of the adaptive and the linear DI-controller in task 2, a circle in the $U_g - W_g$ plane. The resulting responses of U_g vs. W_g are shown over the first cycle. The adaptive controller is chosen as in equations (44)–(47) with the trim estimate $\hat{d}$. The DI controller includes an integrating action. 8

8 Comparison of the adaptive and the linear DI-controller in task 2, a circle in the $U_g - W_g$ plane. The resulting responses of U_g vs. W_g are shown over the eighth cycle. The adaptive controller is chosen as in equations (44)–(47) with the trim estimate $\hat{d}$. The DI controller includes an integrating action. 9

9 Comparison of the adaptive and the linear pole-placement controller in task 3, steps in vertical flight. The resulting responses of w versus time are shown for 0 to 120 seconds, with adaptation stopped at 80s. The adaptive controller is chosen as in section 3. 10

10 Comparison of the adaptive and the linear pole-placement controller in task 3, steps in vertical flight. The resulting responses of u versus time are shown for 0 to 120 seconds, with adaptation stopped at 80s. The adaptive controller is chosen as in section 3. 11

11 Comparison of the adaptive and the linear pole-placement controller in task 4, a coordinated turn. The resulting responses of X_g vs. Y_g are shown over the first cycle. The adaptive controller is chosen as in section 3. 12

12 Comparison of the adaptive and the linear pole-placement controller in task 4, a coordinated turn. The resulting responses of X_g vs. Y_g are shown after adaptation has been stopped. The adaptive controller is chosen as in section 3. 13

Task	*Advantages of Adaptive Controller*	*Figure No.*
1. Step changes in forward velocity	Low steady state error, improvement in transients over time, little overshoot, good learned performance after adaptation is stopped.	Figures 3–5
2. Sinusoidal forward velocity command	Low steady state error, low transients, good learned performance after adaptation is stopped for frequencies different from training set.	Figures 7, 8
3. Step changes in vertical velocity	Low steady state error, low transients and improvement in transients over time, little overshoot, good learned performance	Figures 9, 10
4. Coordinated turn	Low transients, smaller tracking error, good learned performance	Figures 11, 12

Table 1: Summary of numerical simulation tasks.

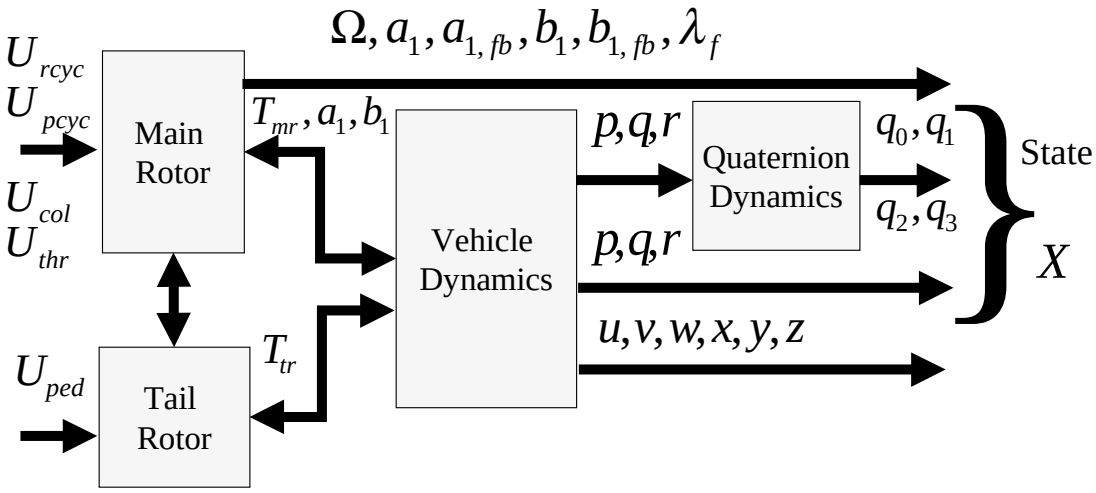

Figure 1: Schematic of helicopter dynamics

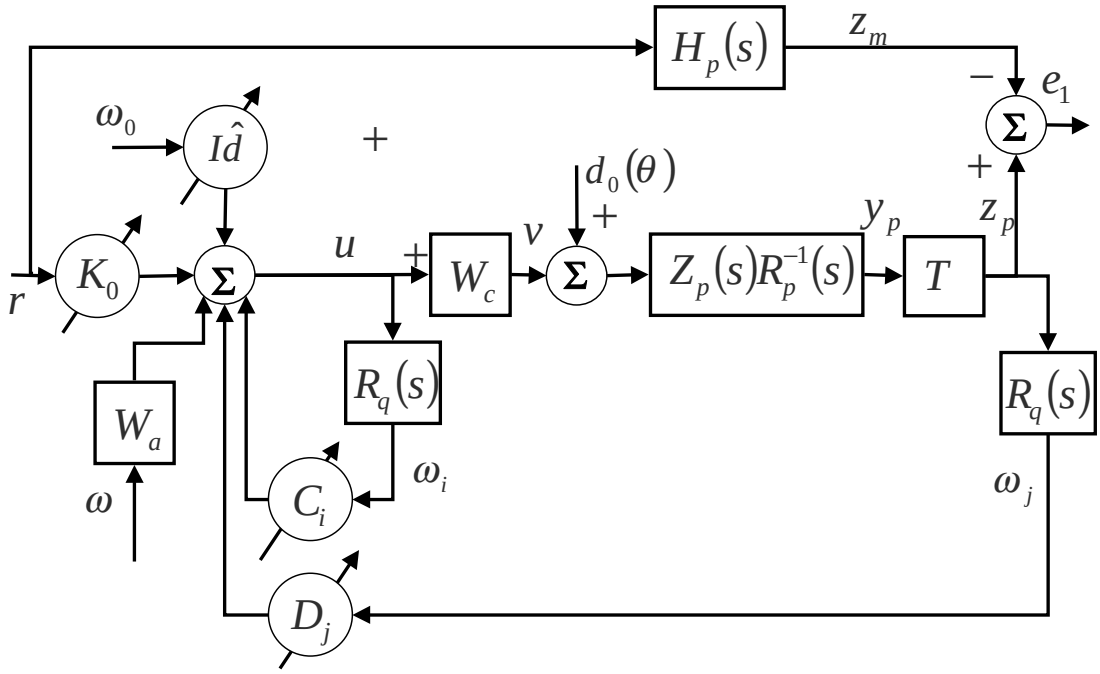

Figure 2: The multivariable plant with the proposed adaptive controller

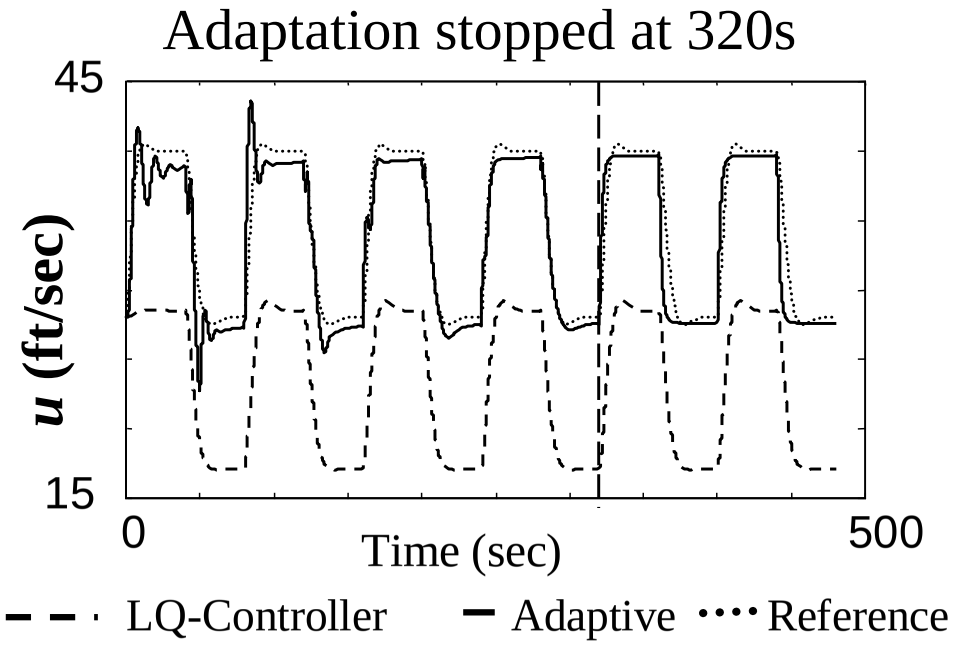

Figure 3: Comparison of the adaptive and the linear LQ-controller in task 1, step changes in forward flight velocity. The resulting responses of u versus time are shown from 0 to 500 seconds, with adaptation stopped at 320s. The adaptive controller is chosen as in equations (44)–(46) but with no trim estimate.

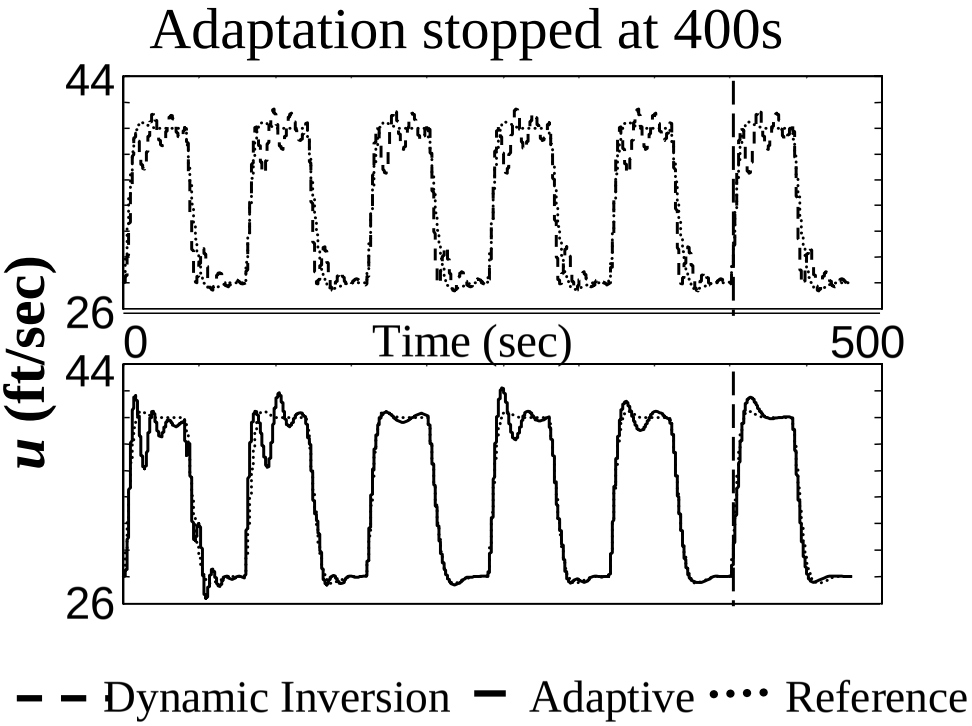

Figure 4: Comparison of the adaptive and the linear DI-controller in task 1, step changes in forward flight velocity. The resulting responses of u versus time are shown from 0 to 500 seconds, with adaptation stopped at 400s. The adaptive controller is chosen as in equations (44)–(47) with the trim estimate $\hat{d}$. The DI controller includes an integrating action.

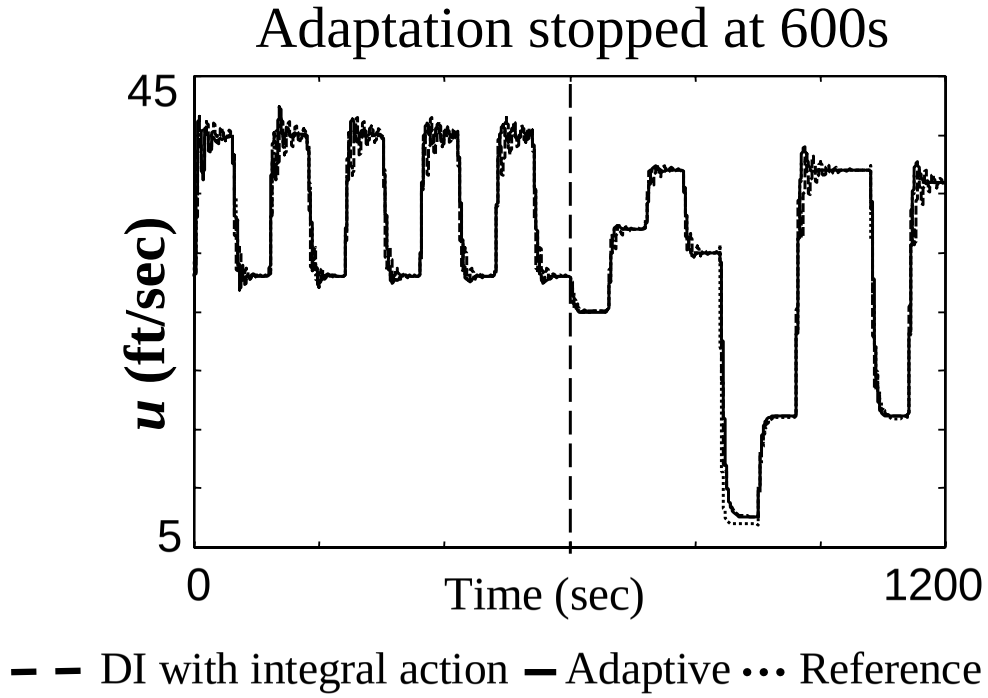

Figure 5: Comparison of the adaptive and the linear DI-controller in task 1, for random step changes in forward flight velocity after a certain time. The resulting responses of u versus time are shown from 0 to 1200 seconds, with adaptation stopped at 600s. The adaptive controller is chosen as in equations (44)–(47) with the trim estimate $\hat{d}$. The DI controller includes an integrating action.

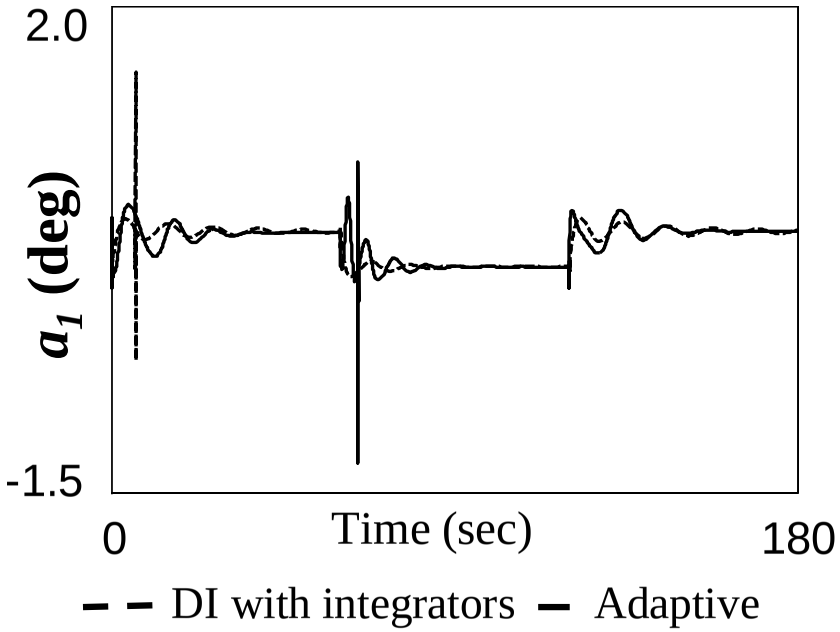

Figure 6: Comparison of the adaptive and the linear DI-controller in task 1, for step changes in forward flight velocity. The corresponding control input, a_1, which is the main rotor pitch flapping is shown versus time for the two controllers from 0 to 180 seconds, which corresponds to the first three cycles. The adaptive controller is chosen as in equations (44)–(47) with the trim estimate $\hat{d}$. The DI controller includes an integrating action.

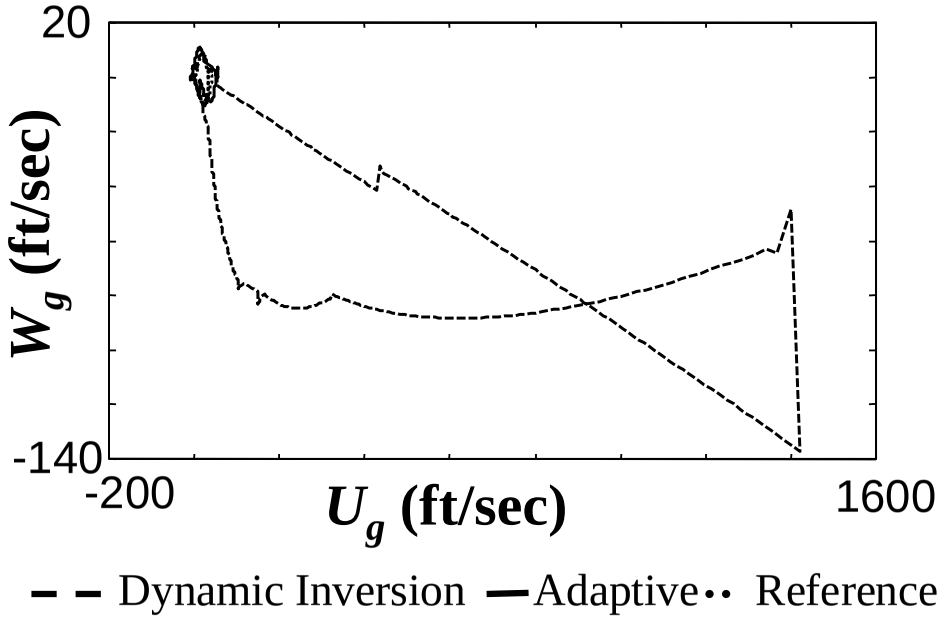

Figure 7: Comparison of the adaptive and the linear DI-controller in task 2, a circle in the $U_g - W_g$ plane. The resulting responses of U_g vs. W_g are shown over the first cycle. The adaptive controller is chosen as in equations (44)–(47) with the trim estimate $\hat{d}$. The DI controller includes an integrating action.

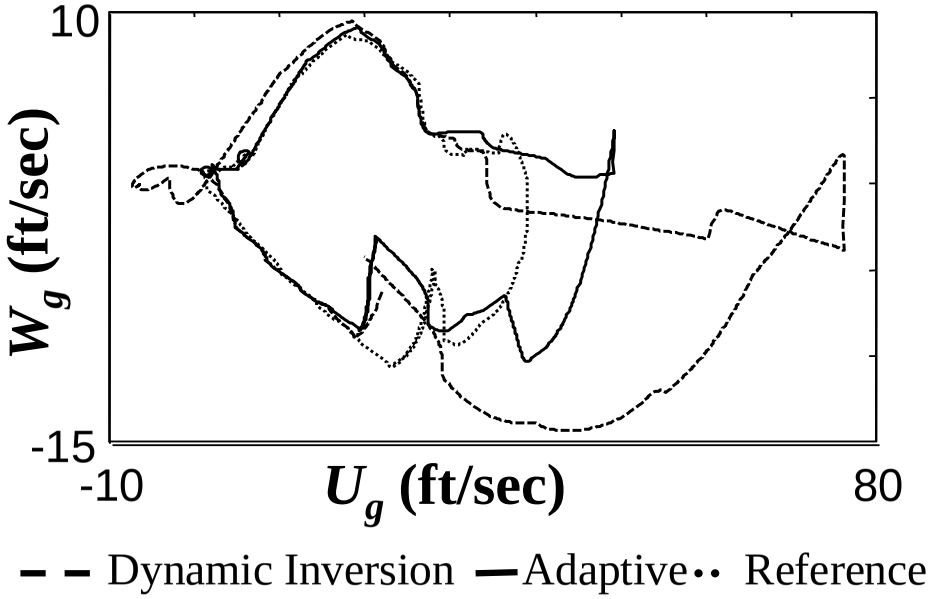

Figure 8: Comparison of the adaptive and the linear DI-controller in task 2, a circle in the $U_g - W_g$ plane. The resulting responses of U_g vs. W_g are shown over the eighth cycle. The adaptive controller is chosen as in equations (44)–(47) with the trim estimate $\hat{d}$. The DI controller includes an integrating action.

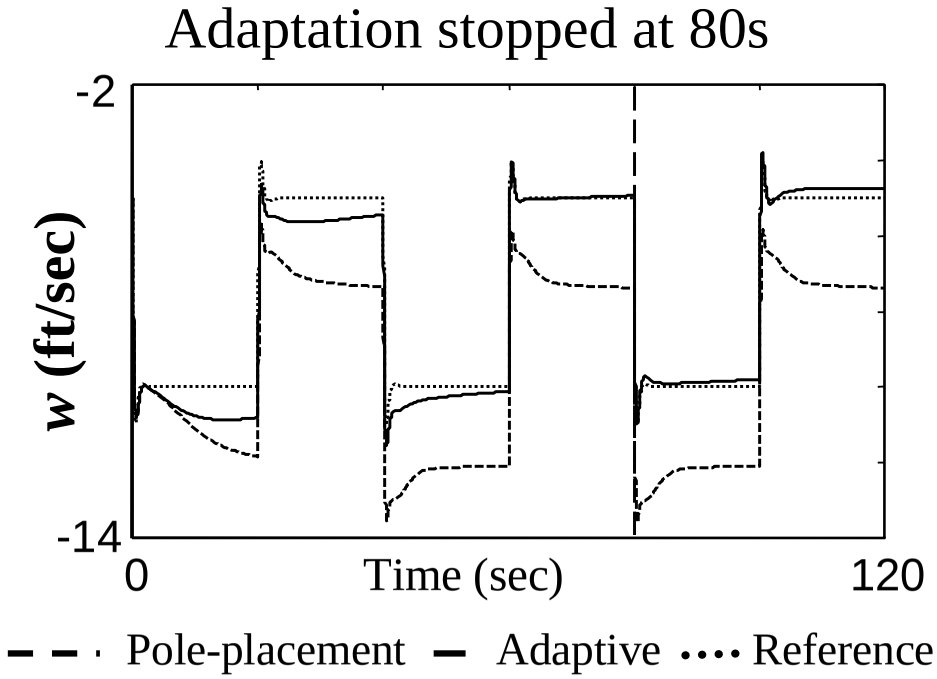

Figure 9: Comparison of the adaptive and the linear pole-placement controller in task 3, steps in vertical flight. The resulting responses of w versus time are shown for 0 to 120 seconds, with adaptation stopped at 80s. The adaptive controller is chosen as in section 3.

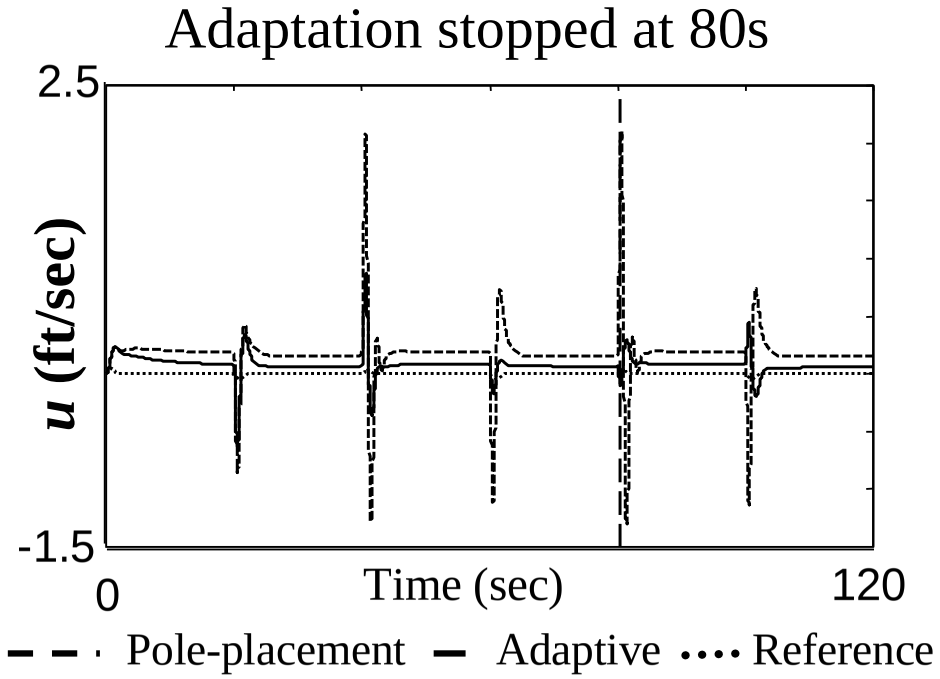

Figure 10: Comparison of the adaptive and the linear pole-placement controller in task 3, steps in vertical flight. The resulting responses of u versus time are shown for 0 to 120 seconds, with adaptation stopped at 80s. The adaptive controller is chosen as in section 3.

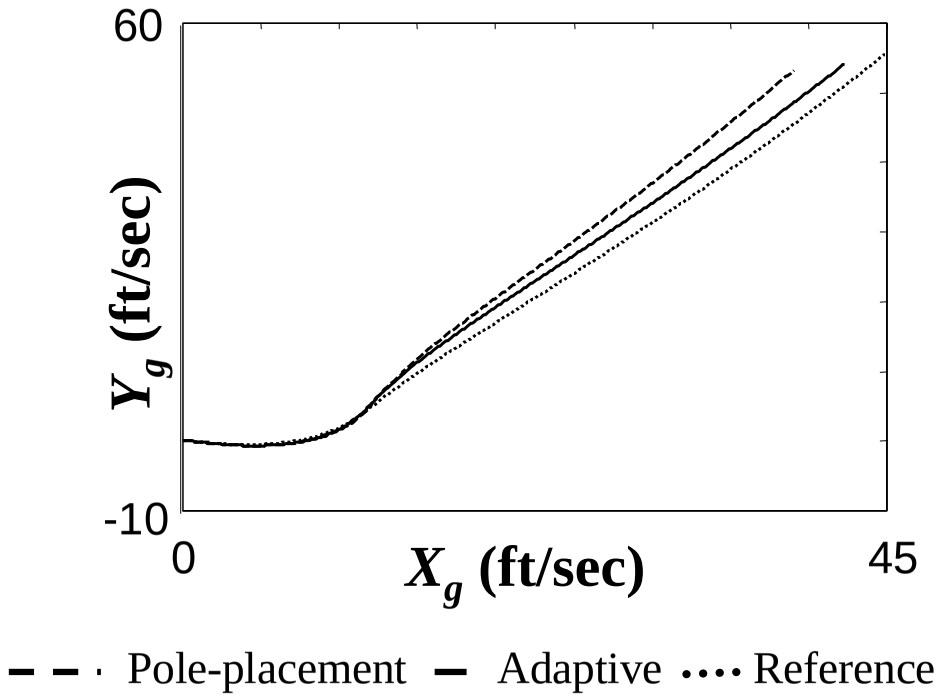

Figure 11: Comparison of the adaptive and the linear pole-placement controller in task 4, a coordinated turn. The resulting responses of X_g vs. Y_g are shown over the first cycle. The adaptive controller is chosen as in section 3.

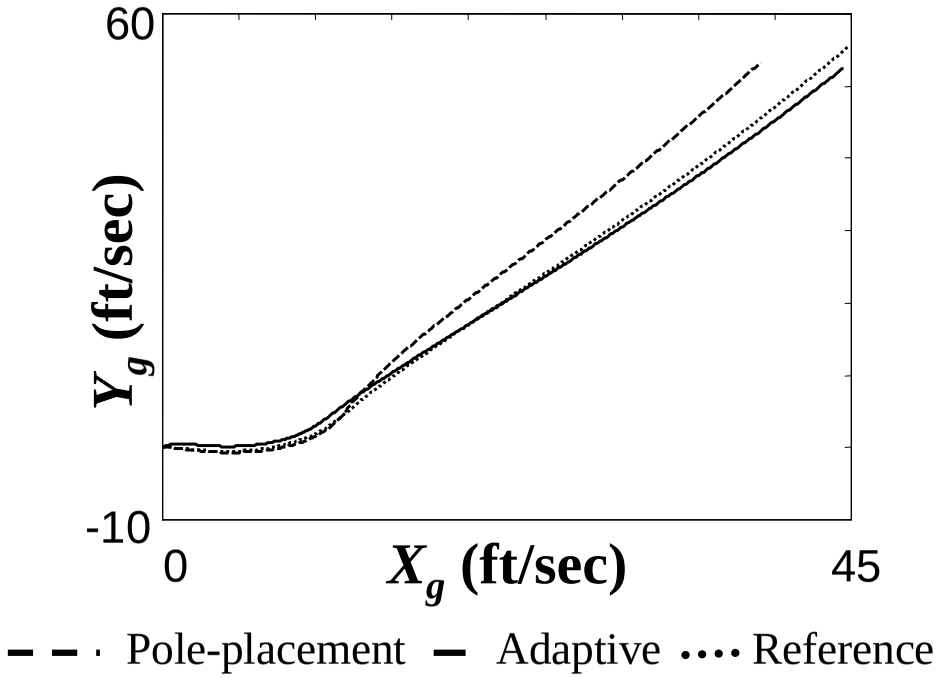

Figure 12: Comparison of the adaptive and the linear pole-placement controller in task 4, a coordinated turn. The resulting responses of X_g vs. Y_g are shown after adaptation has been stopped. The adaptive controller is chosen as in section 3.